# Evidence of Ferrimagnetism in Fe-Doped CdSe Quantum Dots

Jasleen K. Bindra,[†,‡] George Kurian,[§] Jonathan H. Christian,[†] Johan Van Tol,[‡] Kedar Singh,[∥] Naresh S. Dalal,[†,‡] Mogus D. Mochena,[§] Sebastian A. Stoian,[⊥] and Geoffrey F. Strouse[*,†]

[†]Department of Chemistry and Biochemistry, Florida State University, Tallahassee, Florida 32306, United States
[‡]National High Magnetic Field Laboratory, Florida State University, Tallahassee, Florida 32310, United States
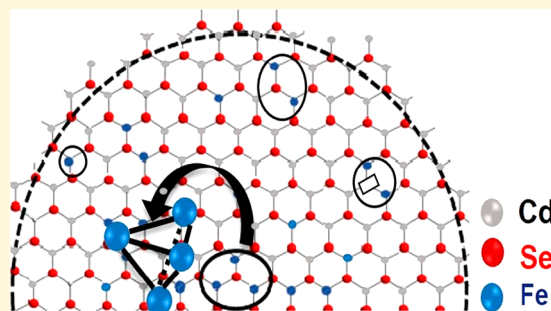[§]Department of Physics, Florida A&M University, Tallahassee, Florida 32307, United States
[∥]School of Physical Sciences, Jawaharlal Nehru University, New Delhi 110067, India
[⊥]Department of Chemistry, University of Idaho, Moscow, Idaho 83844, United States

**S** *Supporting Information*

**ABSTRACT:** Two interacting spin sublattices are observed for 5.1 nm Fe (4.6%) CdSe quantum dots giving rise to a superparamagnetic material with a blocking temperature of ∼90 K. The field- and temperature-dependent $^{57}$Fe Mössbauer spectra reveal that the observed magnetic properties arise from the antiparallel alignment of two dissimilar, Fe(III)-based spin−lattices. Comparison of the experimental data with density functional theory calculations suggests the formation of an ordered minor and major spin−lattice within the quantum dot (QD) can be ascribed to the antisite pair formation of the Fe(III) centers around a cadmium vacancy.

The ability to intentionally incorporate a guest ion into a quantum dot (QD) lattice has been demonstrated using prenucleated clusters[1−3] and by diffusion doping.[4−7] The stochastic incorporation of isovalent (M(II)) and aliovalent (M(III), M(I)) metal ion guest ions into binary QDs, while challenging, can lead to immensely tunable materials.[8−11] In such QDs, emergent electronic,[12−14] plasmonic,[15−18] optical,[19−21] and magnetic[22−31] properties are observed due to the formation of subgap donor states in the electronic band structure. When the guest ion is magnetic, dilute magnetic semiconductor quantum dots (DMSQDs) can be prepared where the exchange interactions are influenced by quantum confinement.[23−29] Isovalent substitution by Mn(II) results in magnetic exchange interactions moderated by the presence of carriers associated with the surface of the QD.[26] While many of the studies to date have focused on isovalent doping, aliovalent ion doping with Cu(I), Cr(III), Fe(III), and Eu(III) has also been reported in the literature. It has been suggested that such aliovalent ion clusters allow charge balance by the formation of antisite dimer pair inclusions ($M_2Se_3$) in the QD lattice.[32−35]

Iron is an interesting guest metal for a II−VI semiconductor QD, as it is capable of incorporating as isovalent (Fe(II)) or aliovalent (Fe(III)) and may occupy either the tetrahedral cation site or the octahedral hole in a II−VI lattice. The presence of iron guest ions was reported to lead to room-temperature ferromagnetism (RT-FM) in FeCdSe[36] and FeZnO[37,38] QDs. In FeZnO, the RT-FM was assigned by electronic structure calculations to formation of a half-metallic system.[39] In our recent study on FeZnSe QDs, a priori DFT calculations revealed the Fe(III) centers localize as antisites,

forming ferrimagnetic spin clusters within the QD lattice. The antisite pairing results in complex antiferromagnetic−ferromagnetic interactions accounting for the observed RT-FM behavior.[35] In analogy to the results on FeZnSe QDs, phase segregation arising from the low solubility of Fe(III) centers in II−VI lattices has been shown to produce local spin clusters in single-crystal Fe-doped ZnO.[40]

This work was undertaken to (i) probe the oxidation state and the preferred site occupied by the Fe dopant in the CdSe lattice; (ii) analyze the local magnetic exchange interactions between dopant ions; and (iii) use density functional theory (DFT) to assess the nature of the exchange interactions between two dopant sites and how these are affected by changes in site occupancy and internuclear distance. In this Article, we report on the experimental data and DFT calculations of a spherical $5.1 \pm 0.7$ nm Fe(III)-CdSe QD. From the fitting of the Mössbauer data at low $T$, the Fe is incorporated at 4.6%, and the oxidation state is 75% Fe(III) and 25% as a disordered Fe center that cannot be definitively assigned as Fe(III) or Fe(II) by Mössbauer spectroscopy. The Fe(III) consists of two ordered spin sublattices that are magnetically coupled. The field-dependent Mössbauer spectra recorded at 4.2 K reveal a field-dependent first-order FM− AFM (Type II) metamagnetic transition. Temperature- and field-dependent DC-magnetic susceptibility measurements confirm that the FeCdSe QDs exhibit a superparamagnetic
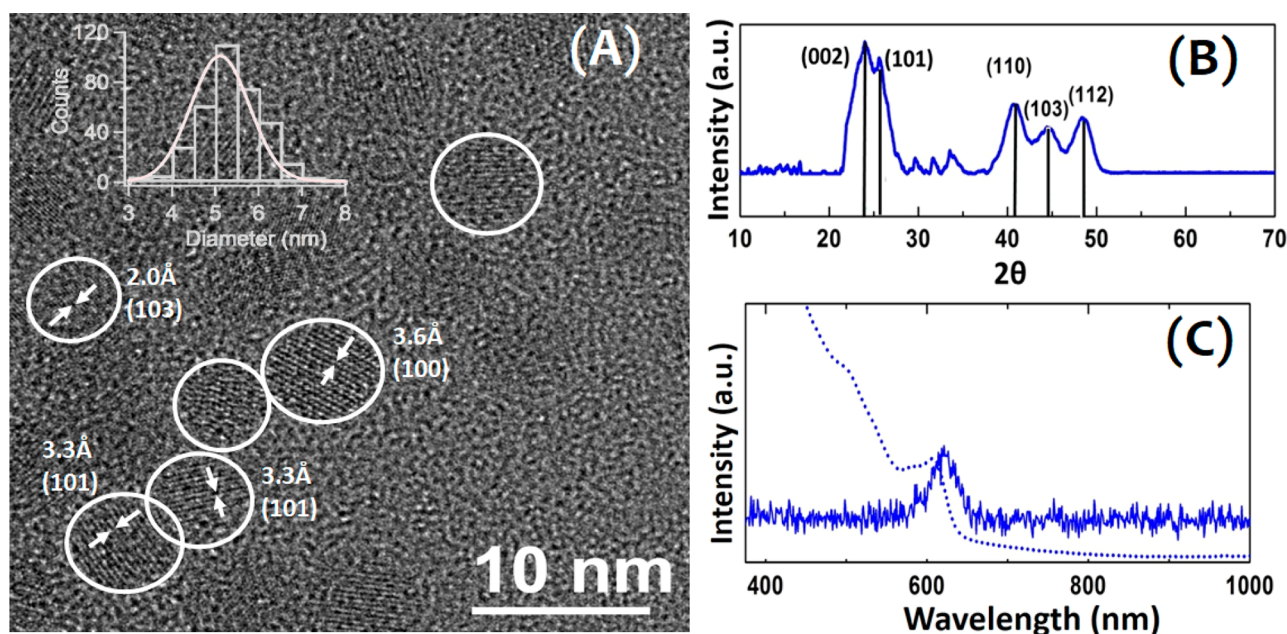
**Figure 1.** (A) TEM micrograph with selected 4.6% FeCdSe QDs circled for easy identification. Lattice *d*-spacing is indicated in the image size fringe analysis with *d*-spacing. QD size distribution from TEM analysis of 300 QDs indicating the size is 5.10 ± 0.66 nm is shown in inset. (B) Powder X-ray diffraction (Cu K$\alpha$), and (C) optical absorption (dashed line) and photoluminescence (solid line) spectra of 4.6% FeCdSe QDs.

(SPM) transition at 90 K with a low coercivity of 800 Oe at 5 K. This transition is assigned as arising from magnetic interactions between a major and minor spin component associated with antisite pairing of aliovalent ions generating a nucleated center within the QD. DFT-VASP calculations were performed to develop a geometric spin model, to explain the observed temperature- and magnetic-field-dependent magnetic behavior. The DFT calculations support antisite pair formation with a Cd vacancy ($V_{Cd}$) to compensate charge imbalance resulting in two distorted tetrahedral sites for the Fe centers that are antiferromagnetically (AFM) coupled. The antisite pair formation appears to produce an ordering in the lattice when aliovalent ions are incorporated. The results support our previous studies on Fe-doped ZnSe QDs[35] where RT-FM arises through phase segregation of dopant ions. This phase segregation leads to the formation of local spin clusters within a quantum confined lattice.

## RESULTS AND DISCUSSION

**Preparation and Characterization of FeCdSe.** Spherical 5.10 ± 0.66 nm FeCdSe passivated by hexadecylamine was isolated from the solvothermal synthesis through the aggregated growth through cluster reformation of $Li_4[Se_4Cd_{10}(SC_6H_5)_{16}]$ in the presence of $FeCl_2$.[1] The reactions are carried out at 220 °C to ensure no S-ion incorporation arising from surface-mediated thiophenol decomposition pathways.[41] Fe incorporation at 4.6 wt % is confirmed by inductively coupled plasma mass spectrometry (ICP-MS) and corresponds to ~20 Fe atoms per CdSe QD on average. The use of a molecular cluster as a single-source precursor to achieve guest ion incorporation in II−VI QDs has been previously reported for a wide range of isovalent and aliovalent cation substitution reactions.[1−3,24−27,32]

The size and the size distribution of the isolated QDs were measured by TEM image analysis of 300 QDs (Figure 1A). As shown in Figure 1B, the formation of a wurtzite crystal motif was observed by powder X-ray diffraction (JCPDS card 77-

23077). Scherrer analysis of the (100) pXRD, Figure 1B, agrees with the TEM size measurement. TEM fringe analysis confirms the assignment of wurtzite with observed *d*-spacings of 0.20 nm for the (103) plane, 0.36 nm for the (100) plane, and 0.33 nm for the (101) plane. No evidence of impurity phase contamination by $Fe_xSe_y$, $FeSe_xO_y$, $Fe_xO_y$, or $CdFe_2O_4$ is observed in the pXRD data or in the TEM fringe analysis. In the pXRD the (100) peak is not observed to shift due to Fe incorporation into the lattice. The lack of a shift is inconsistent with Vegard law analysis for substitutional doping[42] and may indicate phase segregation or dimer pair formation as reported in Cu(I), Cr(III), and Eu(III) incorporation into CdSe QDs.[32−34] The formation of dimers or larger clusters was postulated to reduce lattice strain and compensate for charge imbalance in FeZnSe QDs.[35] Figure 1C shows the optical absorption and photoluminescence (PL) data collected for the FeCdSe dissolved in toluene. The optical absorption spectra have clearly defined excitonic features, while the PL arises from CdSe bandgap emission but is strongly quenched (<1% QY, quantum yield), a common feature in transition-metal-doped (TM-doped) CdSe QDs.[42]

**HF-EPR Spectroscopy.** The iron site can incorporate at a substitutional site on a $T_d$ cation site or interstitial at an Oh hole in the lattice. In addition, Fe(II) and Fe(III) are able to be incorporated into II−VI binary semiconductors.[30,31,35,36,43,44] Figure 2 shows the high-frequency EPR (HF-EPR) spectrum recorded at 240 GHz, 290 K. The EPR spectra consist of a single asymmetric resonance centered at $g = 2.018 ± 0.03$. The spectrum could be simulated considering a single Fe(III) species with $S = 5/2$ including spin-dipolar broadening due to Fe(III)−Fe(III) spin interactions within the lattice. The observed *g*-value and the lack of fine structure (D) are consistent with reported *g*-values for Fe(III) incorporation at a $T_d$ substitutional ion site with observed line broadening arising from Fe(III)−Fe(III) dipolar interactions with lattice.[30,31,36,43,44] The observed asymmetric line-shape is ascribed to the deviation from $T_d$ symmetry.
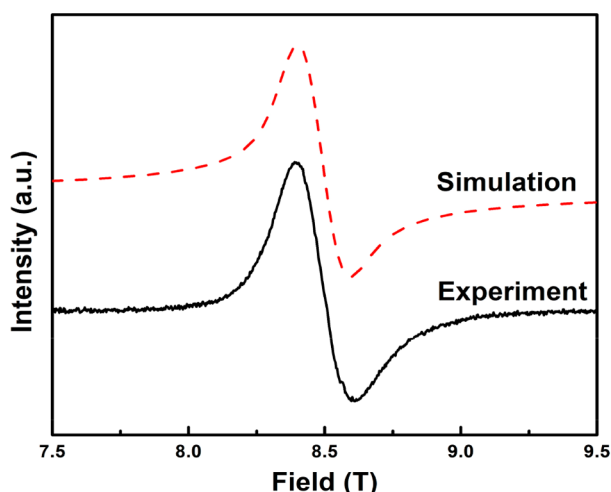
**Figure 2.** Experimental (black) and simulated (red) HF-EPR spectrum recorded at 240 GHz, 290 K for the 4.6% Fe-doped CdSe QDs.

## $^{57}$Fe Mössbauer Spectroscopy.

Mössbauer spectroscopy was utilized to obtain a definitive assignment of the oxidation state of the Fe dopant sites. Figure 3A,B shows a series of field- and temperature-dependent $^{57}$Fe Mössbauer spectra recorded for FeCdSe QDs dispersed in eicosane. Eicosane was used to reduce the complications arising from QD−QD interactions and to impede the field-induced reorientation of QDs. The field-dependent Mössbauer spectra were measured with the magnetic field applied parallel to the propagation direction of the 14.4 keV γ rays.

The field-dependent, $^{57}$Fe Mössbauer spectra recorded at 4.2 K, including the zero-field spectrum, were best simulated considering three spectral components. Two components belong to a magnetically ordered, Fe(III)-based phase that accounts for ∼75% of the Fe present in the sample. The third is associated with a disordered phase that is best described using parameters that are suggestive of iron(II) ions.[47] A summary of the parameter values used to simulate the zero-field spectrum recorded at 4.2 K is provided in Table 1. The disordered phase might have arisen either from heterogeneous Fe(III) centers at the surface, a surface-localized oxide phase, or, possibly, Fe(II) originating from the formation of surface defect centers. In a recent report, the presence of both Fe(II) and Fe(III) sites was observed in FeZnO QDs. In this case the Fe(II) was associated with the photoexcited population of a low-lying charge transfer electronic state that could be reversibly populated.[31]

The nature of the magnetically ordered phase was assessed by analyzing the field- and temperature-dependent data (Figure 3, Supporting Information Figures S1 and S2). In
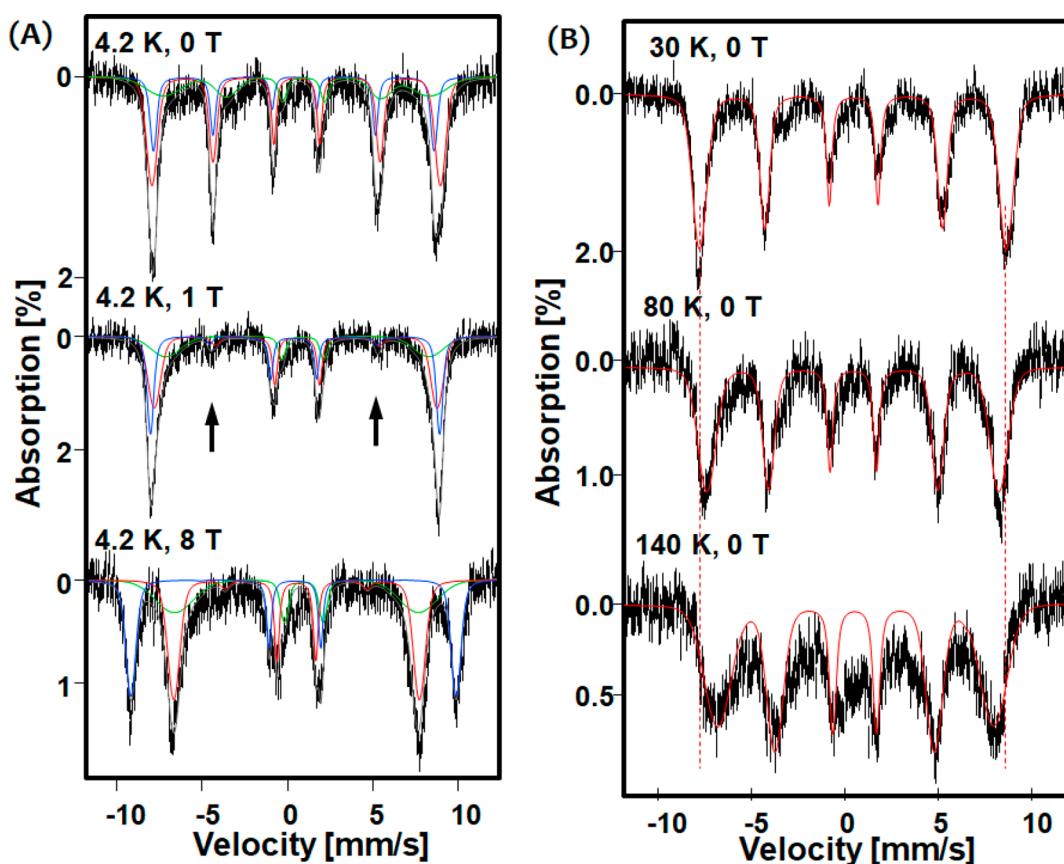


**Figure 3.** (A) Variable-field, 4.2 K $^{57}$Fe Mössbauer spectra and (B) variable-temperature, zero-field spectra recorded for the $^{57}$FeCdSe QDs. The 4.2 K spectra are deconvoluted into three distinct components. Two components belong to a magnetically ordered phase (red and blue), and the third is magnetically disordered (green), see text. The vertical arrows of the 1 T, 4.2 K spectrum highlight the field-induced decrease in the intensities of the $\Delta m_I = 0$ lines, i.e., the occurrence of a metamagnetic transition. The solid red lines of the temperature-dependent spectra are simulations obtained considering a single spectral component that accounts for ∼75(5)% spectral area. The vertical dotted lines illustrate the temperature-induced change in the observed magnetic hyperfine splitting.

**Table 1. Hyperfine Splitting Parameters Derived from the Analysis of the 4.2 K Spectra Recorded for the FeCdSe QDs**

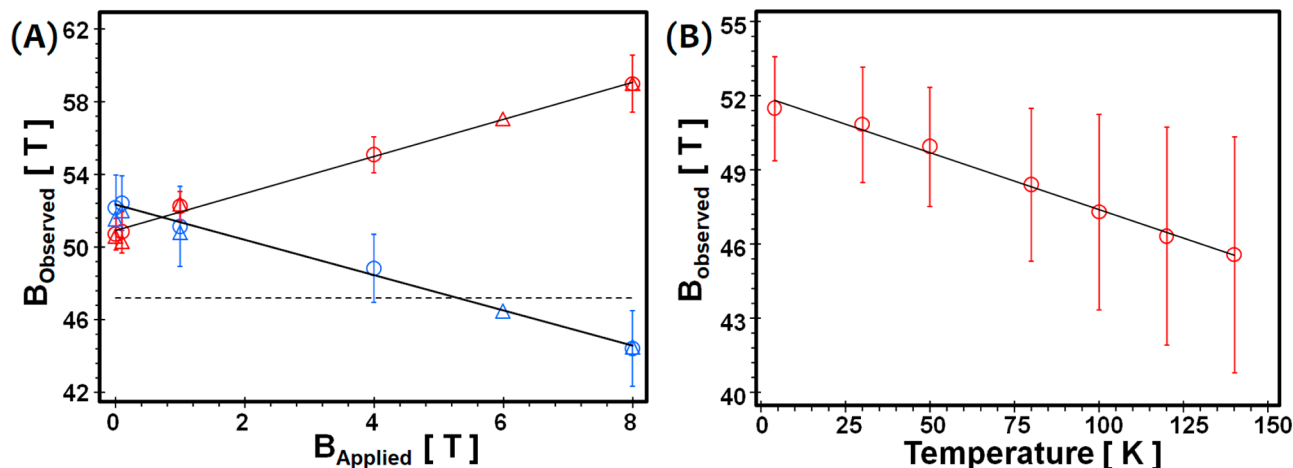| phase | component | $\delta$ [mm/s] | $\varepsilon$ [mm/s] | $B_0$ [T] | $dB$ [T] | % |
|---|---|---|---|---|---|---|
| ordered | major | 0.48(1) | −0.05(5) | 52.3(8) | 1.8(5) | 42(2) |
| | minor | 0.36(2) | 0.05(5) | 50.9(5) | 1.2(2) | 28(2) |
| disordered | n.a.[a] | 0.6(1) | −0.4(1) | 47.2(9) | 6(2) | 25(3) |

[a] n.a.: not applicable.



**Figure 4.** (A) 4.2 K, field-induced and (B) zero-field, temperature-dependent changes in the magnetic hyperfine splitting observed for the $^{57}$FeCdSe QDs (O). The solid lines are linear fits obtained using eqs 2 and 3, see text. The dotted horizontal line corresponds to the observed hyperfine splitting of the magnetically disordered phase. The error bars account for the fwhm of the hyperfine field distribution determined from the simulations of the experimental data.

this case, it was imperative to consider the situation of magnetic QDs in contact with a neighboring magnetic QD. The energy of the system with respect to the QD volume (V) can be written in the presence of an applied field $\mathbf{B}_{\text{app}}$ as

$$E = UV\sin^2\theta + MV\mathbf{B}_{\text{app}}\cos\varphi + K_{\text{ex}}M\mathbf{M}_c\cos\omega \quad (1)$$

The first term describes the magnetic anisotropy where $U$ is the magnetic anisotropy energy constant, and $\theta$ describes the angle between the easy axis of magnetization and the magnetization vector of the QD. Since the FeCdSe QDs are ferrimagnetic $U$ is a composite quantity that accounts for the anisotropies of both magnetic sublattices and the exchange interaction between them. The second term accounts for the Zeeman energy of the particle such that $MV$ is the magnetic moment of the particle, and $\varphi$ describes the angle between its magnetization vector and the applied field, $\mathbf{B}_{\text{app}}$. Finally, the third term describes the exchange interaction of the QD under consideration with a neighboring particle with a magnetization $\mathbf{M}_c$. For this term, $\omega$ describes the angle between the magnetization vectors of the two particles. The Zeeman interaction of ferro- or ferrimagnetic QDs is expected to be considerably larger than both the magnetic anisotropy and the interparticle exchange interactions even for fields as small as 1 T.

*Field-Dependent Mössbauer Data.* The field-dependent Mössbauer spectra (Figure 3A, Supporting Information Figure S1) show that applying a magnetic field leads to the disappearance of the second and fifth lines and to a clearly observed separation of the sextet observed in zero-field into two individual components. Thus, the 8 T (4.2 K) spectrum of Figure 3A clearly shows two patterns with unequal spectral areas and unique magnetic hyperfine splittings. The observed

field dependence can be rationalized using the approach of Mørup et al.[48]

$$|\mathbf{B}_{\text{obs}} - \mathbf{B}_{\text{app}}| \cong B_0\left(1 - \frac{k_B T}{MV\mathbf{B}_{\text{app}}}\right) \quad (2)$$

where $B_0$ is the internal field observed in zero applied field, $\mathbf{B}_{\text{app}}$ is the applied magnetic field, $\mathbf{B}_{\text{obs}}$ is effective magnetic hyperfine field observed for a particular applied field value, $MV$ is the magnetic moment of the particle, and $k_B T$ is Boltzmann energy. The $\mathbf{B}_{\text{obs}}$ and $B_0$ values of eq 2 could be easily extracted from the experimental magnetic hyperfine splitting using the WMOSS software (See Co., formerly Web Research Co., Edina, MN; see the Experimental Section). Plotting the values of $\mathbf{B}_{\text{obs}}$ vs $\mathbf{B}_{\text{app}}$ from 0 to 8 T in Figure 4A confirms that the observed hyperfine splitting is linearly dependent on the applied field with a slope of +1.02 for the major and −0.97 for the minor component. While the hyperfine splitting of the major component decreases with the applied field, for the minor component the hyperfine splitting increases with the applied field.

The relative intensities of the six lines of a spectrum originating from a random distribution of Fe sites with uniaxial magnetic properties, such as that observed in zero-field, are given by 3:$x$:1:1:$x$:3 where $x = 2$. However, for a finite angle $\theta$ between the hyperfine field and the $\gamma$ rays $x = 4\sin^2\theta/(1 + \cos^2\theta)$. Thus, the change in the intensities of the observed resonances originates from a field induced-alignment of the local Fe moments with the applied field, i.e., metamagnetic transition. The separation of the magnetic hyperfine splitting pattern into two unequal components is indicative for the presence of two distinct magnetic sublattices. For high-spin Fe(III) ions the hyperfine coupling tensor that describes the interaction between the nuclear and electronic spins is
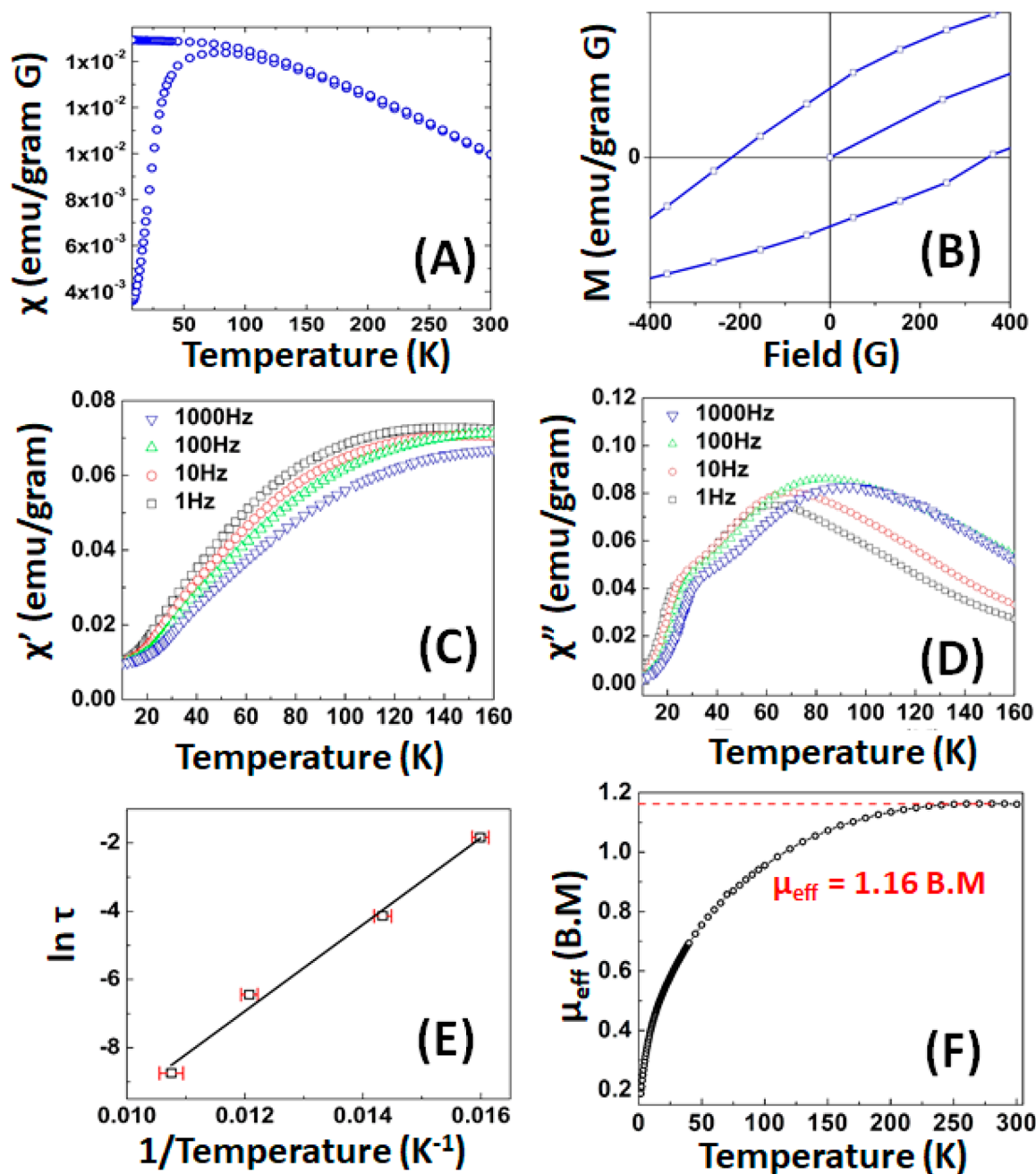
**Figure 5.** DC-SQUID susceptibility measurements, (A) field cooled (FC) and zero-field cooled (ZFC), (B) magnetization, AC-susceptibility (C) in-phase, and (D) out-of-phase plots, (E) Arrhenius and (F) $\mu_{eff}$ plots for 5 nm, 4.6% FeCdSe QDs.

expected to be essentially isotropic and to be negative. Therefore, together with the change in the intensities of the observed $\Delta m_I = 0$ resonances (the two middle, second, and fifth lines), the decrease in the hyperfine splitting demonstrates that the magnetic moment of the larger sublattice is aligned parallel to the applied field. At the same time the field-induced increase in the splitting of the minor component shows that the magnetic moment of this sublattice is found antiparallel to the applied field. In turn, these observations clearly demonstrate that a ferrimagnetic ordered phase with a collinear spin arrangement exists within the FeCdSe QD.

*Temperature-Dependent Mössbauer Data.* The temperature-dependent behavior of the Mössbauer spectra at 0 T is shown in Figure 3B and Supporting Information Figure S2. The sextet observed at 4.2 K broadens with increasing

temperature but does not collapse to a doublet over the temperature range measured. The observed, temperature-dependent behavior is typical of magnetic nanoparticles involved in long-range dipolar interactions, where magnetically interacting nanoparticles have been reported to exhibit a gradual broadening of the observed resonances with increasing temperature.[45,46] The broadening is accounted for by considering the spontaneous fluctuations of the magnetization between the two orientations parallel to the easy axis, i.e., superparamagnetic relaxation. These fluctuations are known as collective magnetic excitations and lead at low temperatures to a linear decrease in the observed magnetic hyperfine splitting.

The persistence of the sextet at room temperature is surprising, as a collapse to a doublet in Fe-doped $In_2O_3$ a doublet has been reported.[49] For a superparamagnetic system a

doublet arises when the magnetization of the individual nanoparticles or QDs exhibits a flip rate higher than the nuclear Larmor precession. This leads to the averaging out of the magnetic hyperfine interactions and, thus, to a two-line spectrum, that is, a quadrupole doublet. For the FeCdSe QD sample investigated here no doublet could be detected even at 200 K. The lack of a quadrupole doubled together with the temperature-induced decrease in the magnitude of the magnetic hyperfine splitting can be rationalized by considering the effects of interparticle magnetic interactions. A review of eq 3 suggests that to a first approximation these interactions lead to an effective increase in the energy barrier and thus to a lower relaxation rate.

$$\mathbf{B}_{obs} \cong B_0\left(1 - \frac{k_B T}{2UV + K_{ex} M \mathbf{M}_c}\right) \tag{3}$$

In Figure 4B, a plot of $|\mathbf{B}_{obs}|$ vs $T$ allows the sum of exchange and magnetic anisotropy $(2UV + K_{ex}M\mathbf{M}_c)$ to be evaluated. The slope of the temperature-induced change in the magnetic hyperfine splitting is −46.1 mT/K yielding a value for the effective energy barrier of the system as defined by the sum of the exchange and magnetic anisotropic energies of ∼15 cm$^{-1}$. Although the investigation of a series of samples with different QD concentrations might allow for the determination both of the magnitude of interparticle exchange interactions and of the anisotropic exchange constants, the high nonresonant absorption of the 14.4 keV by the heavy Cd and Se nuclei renders such systematic studies quite difficult.

**Magnetic Properties of FeCdSe.** To probe the spin dynamics of the anticipated Fe(III) clustering AC and DC-magnetic susceptibility and magnetization measurements were performed. The interpretation of the FeCdSe QD field-dependent Mössbauer in terms of a ferrimagnetic material arising from the presence of competing AFM spin sub lattices (type II AFM) would explain the earlier report of RT-FM in FeCdSe without half-metal formation.[36,37] The magnetic properties of the FeCdSe QD were measured by temperature- and field-dependent DC-magnetic susceptibility (Figure 5A,B). The DC-magnetic susceptibility data confirms the FeCdSe sample is a room-temperature magnet (0.001 emu/g). The observation of RT-FM confirms the earlier published reports of FeCdSe QDs.[36] A broad blocking temperature is observed between 90 and 100 K in the ZFC vs FC susceptibility plot. Figure 5B shows the field-dependent magnetic susceptibility at 5 K which exhibits asymmetric hysteresis loops with a coercivity ($H_c$) of 500 G. Plotting the temperature-dependent coercivity (Supporting Information Figure S3) indicates that the hysteresis approaches an asymptote at 90 K. The temperature-dependent hysteresis is consistent with blocking behavior of superparamagnetic (SPM). SPM behavior is confirmed by measuring the frequency-dependent AC-magnetic susceptibility data at 100 Oe (Figure 5C,D). In the AC-susceptibility data an out-of-phase component ($\chi''$) with a frequency-dependent (60−100 K) and a frequency-independent (35 K) feature is observed. The frequency-independent feature at 35 K is only observable in the AC-susceptibility measurement. The frequency-dependent relaxation time vs temperature data analyzed using the Mydosh criteria, $\Phi = \Delta T_f/T_f\Delta(\log \omega)$, yields a value of $\Phi$ of 0.14 confirming the existence of a SPM magnetic phase. In the Mydosh formula $T_f$ is the temperature at which the maximum in $\chi''$ (T) occurs, $\Delta T_f$ is the difference in $T_f$ between frequencies $\omega_i$ and $\omega_f$, and

$\Delta(\log \omega)$ is the difference between the log of the measuring frequencies.[50]

Analysis of the AC-susceptibility data allows us to estimate the energy required to flip the spin in the single-domain materials ($E_a$) and magnetocrystalline anisotropy ($K$) using the Stoner−Wohlfarth theory $E_a = KV \sin^2 \theta$, where $K$ is the magnetocrystalline anisotropy, $V$ is the volume of the QD, and $\theta$ is the angle between the magnetization direction and the easy axis of the QD. As shown in Figure 5E plotting the relaxation lifetime ($\tau$) vs $1/T$ yields the energy barrier for spin relaxation ($E_a$) via the Arrhenius equation, $\tau = \tau_0 \exp\left(\frac{E_a}{k_B T}\right)$, where $\tau_0$ is the characteristic reversal attempt time, and $E_a/k_B$ is the magnetic reversal energy barrier. The average spin relaxation lifetime ($\tau$) can be extracted from the AC-susceptibility data, since $\tau$ is calculated as $1/(2\pi v)$, where $v$ is the frequency of the AC measurement. The high-temperature (300−250 K) fit of $1/\chi$ vs $T$ (Supporting Information Figure S4) yields a Curie constant of 0.19 emu K/g and Weiss temperature of $\theta = -104$ K implying the presence of AFM exchange coupling in the lattice. Obtained value of Curie constant is close to 0.17 emu K/g obtained using $C = 0.125\mu_{eff}^2$. The AFM exchange would explain the asymmetry in the field-dependent susceptibility measurements, as the existence of a coexisting FM and AFM exchange interactions in different domains would yield exchange bias behavior in the data. A fit of $\chi T$ vs $T$ yields a $\mu_{eff}$ value of 1.16 $\mu_B$/ion, Figure 5F, which is lower than the predicted value for a high-spin Fe(III) center on the $T_d$ cation site ($\mu_{eff} = 1.73$ $\mu_B$/ion), implying the presence of considerable AFM interactions in the sample. The observation of an AFM interaction observed in the magnetic susceptibility data suggests that the Fe(III) ions are strongly interacting in the lattice, consistent with the conclusion from the Mössbauer data analysis.

**Origin of the Interacting Magnetic Spin Sublattice.** The spin−spin interactions observed between Fe(III) ions that lead to RT-FM observed in the magnetic susceptibility measurements can be interpreted in terms of formation of antisite iron dimers in the lattice to accommodate charge imbalance. The dimer formation can be realized as follows. We first calculate formation energies with DFT as implemented in the Vienna ab initio simulation package (VASP)[51,52] for four possible formation sites for the Fe(III) ion: an interstitial tetrahedral site, an interstitial octahedral site, a tetrahedral cation site, and a surface $T_d$ cation site.[5] The formation energy is given by $E^{form} = E(SC^*) - E(SC) - \sum_i \Delta n_i\mu_i + q(E_F + E_v + \Delta V)$ where $E(SC^*)$ and $E(SC)$ are the total energies of the supercell with and without the Fe impurity, respectively.[53] The atoms of the nanocluster are grown in a colloid and are considered to be in contact with particle reservoirs of Cd, Fe, and Se. The $\Delta n_i$ in the third term accounts for ions of Cd removed from or Fe added into the cluster, and $\mu_i$ is the chemical potential of each ion species. The last term is included to account for the exchange of electrons between the nanocluster and the electron reservoir. Since the ordered phase consists of only Fe(III), as determined from the Mössbauer spectra, we take $q$ to be the charge of Fe(III). $E_F$ is the Fermi level, $E_v$ is the energy of valence band maximum (VBM), and $V$ is the correction due to the distortion of the VBM due to the charged Fe impurity. Since only one oxidation state of Fe(III) is assumed here, we assume the last term to be almost equal for all the sites and can be ignored in relative energy calculation, and the results are given in Table 2. The results show that site

**Table 2. Relative Formation Energies in $Cd_{90}Se_{90}$**

| sites for Fe | formation energy (eV) |
|---|---|
| interior substitution | −0.269 |
| tetrahedral interstitial | −1.718 |
| octahedral interstitial | −1.762 |
| surface substitution | −4.185 |

occupation at surface is most favorable, followed by interstitial site and least favorable at interior substitution site since it involves the kicking out of Cd for Fe to replace it.

The evolution of ferrimagnetism can be ascribed as follows. The Fe atoms form first on surface sites since the formation energy is the lowest for the surface substitutional sites. These Fe sites are most likely far apart in the diluted concentration range 5−10% for Fe ions in the colloid. To validate this plausible assumption, the structures were optimized for ferromagnetic and antiferromagnetic coupling between two Fe(III) ions with one occupying a substitutional cation site and the second iron occupying an interstitial site. The calculation was performed on multiple distances between two iron centers occupying a cation tetrahedral substitutional site or an octahedral interstitial site situation. The results of the calculations (Table 3) support that AFM interactions between the iron centers are favored, and ferromagnetic coupling is favorable at larger distances.

**Table 3. Magnetic Correlations for Ferromagnetic and Antiferromagnetic Coupling for Two Fe Ions[a]**

| configuration | orientation | distance (nm) | $\Delta E$ (eV) | magnetic moment ($\mu_B$) |
|---|---|---|---|---|
| two-surface tetra substitution $Cd_{88}Se_{90}Fe_2$ | F | 1.00 | 0.000 000 | 9.0344 |
| | AF | 1.00 | 0.005 499 | −0.6648 |
| | F | 1.82 | 0.000 000 | 8.8399 |
| | AF | 1.82 | 0.008 445 | −0.7089 |
| surface substitution and interstitial $Cd_{89}Se_{90}Fe_2$ | F | 0.80 | 0.000 000 | 8.0245 |
| | AF | 0.80 | 0.034 185 | −0.5629 |
| surface substitution and interstitial $Cd_{87}Se_{90}Fe_2$ | F | 0.45 | 0.012 940 | 7.0229 |
| | AF | 0.45 | 0.000 000 | 1.2500 |
| interior substitution and interstitial $Cd_{87}Se_{90}Fe_2$ | F | 0.28 | 0.269 694 | 7.8510 |
| | AF | 0.28 | 0.000 000 | 0.7304 |

[a]The lower energy of the two orientations is taken as zero energy.

In Figure 6, two irons are shown occupying two substitutional sites (Figure 6A) and an interstitial and substitutional site (Figure 6B). As the nanocrystal is growing iron atoms add to the surface as substitutional ions and can move to a lower energy interstitial site. To see the possibility of the ionic motions, we calculated barrier energies for diffusion of Fe ions from $T_d$ cation site to interstitial site and vice versa as well as from interstitial to interstitial sites using the nudged elastic band method as implemented in VASP with a supercell consisting of 96 atoms as was done in ref 54. The results are consistent with similar results in the reference for diffusion of Ag ions in CdSe[54−56] and are given in Table 4. The results show that the energy barrier is much smaller for motion from

$T_d$ cation site to interstitial than vice versa consistent with similar consideration for silver ions in cation exchange with Cd.[54] When the surface substitutional ion sites become core $T_d$ site due to growth of the cluster, they become unstable and diffuse into interstitial site. A nearby Cd ion can move into the $T_d$ site or it could remain vacant. We ruled out the vacancy formation as it leads to distortion of the lattice and is not consistent with the tetrahedral symmetry. The Fe ion at interstitial site will diffuse to surface via the interstitial route. The 0.28 eV barrier energy is consistent with similar results in fast diffusion.[54−56] The movement of ions to the surface is also consistent with the previous argument for self-purification of quantum dots.[57] The Fe ion that moves out to the surface will couple antiferromagnetically with the Fe ion that has already been formed on the surface. The arrangement is represented by an antisite pair in Figure 6B. The antisite pair assumes a vacancy formation at Cd site ($V_{Cd}$) near the Fe dimers. The $V_{Cd}$ at surface reduces strain in the lattice, providing the attractive Coulomb interaction to anchor the interstitial Fe ion[58] and relax for charge compensation without large distortions to the lattice.

The calculated distortion of the antisite iron dimer around a $V_{Cd}$ site is represented in Figure 7. The $V_{Cd}$ occupies a surface site, and the Fe(III) centers occupy a tetrahedral cation (substitutional) and octahedral (interstitial) site. The Fe ions energetically favor a pseudo-spinel-like arrangement within the hexagonal lattice. When the $V_{Cd}$ sites are in the interior, the interstitial octahedral site moves from its initial position (Figure 6A) by a significantly outward position producing a distorted tetrahedral interstitial site as represented in Figure 6B. In both cases, the Fe(III) ions appear to occupy distorted sites around a $V_{Cd}$, which allows the Fe ion to migrate toward the octahedral interstitial site forming the antisite pair forming a dimer. The antiferromagnetic coupling with $V_{Cd}$ at surface has a lower energy, with a net moment of 1.25 $\mu_B$ resulting in ferrimagnetism, in agreement with our experimental results.

## CONCLUSIONS

This study supports the appearance of RT-FM in FeCdSe QDs arising from formation of competing AFM iron spin sublattices through antisite pairing of Fe(III) centers resulting in a ferrimagnetic interaction. The observed magnetic behavior is reminiscent of the observed AFM−FM exchange interactions between a major and minor spin sublattice in ferrites.[49] In nanoferrites, a mixed-spinel structure leads to anion-mediated superexchange interactions between two magnetic sublattices that correspond to the tetrahedral and octahedral sites and thus to the stabilization of a ferrimagnetic ordered state.[49] The magnitude of the exchange interaction is dependent on the degree of lattice inversion. Considering the close similitude between the spectroscopic behaviors observed for nanosized ferrites[49] and for FeCdSe QDs, we propose that the Fe-doping process leads to the formation of an analogous mixed-spinel phase. Thus, the Fe ions can either displace a Cd(II) cation leading to a substitutional inclusion with a (A) tetrahedral site geometry or, the Fe ions can be incorporated interstitially leading to the formation of a [B] octahedral site. Accordingly, the minor component of the ordered phase of [57]FeCdSe QDs is associated with the (A), and the major component with the [B] sites. Using the relative ratio of the spectral areas determined from the analysis of the 4.2 K spectra, $\alpha = 0.66$, the inversion degree can be determined as $x = (1 − \alpha)/(1 + \alpha) \cong 0.2$. Considering that the Cd(II) cations have a strong
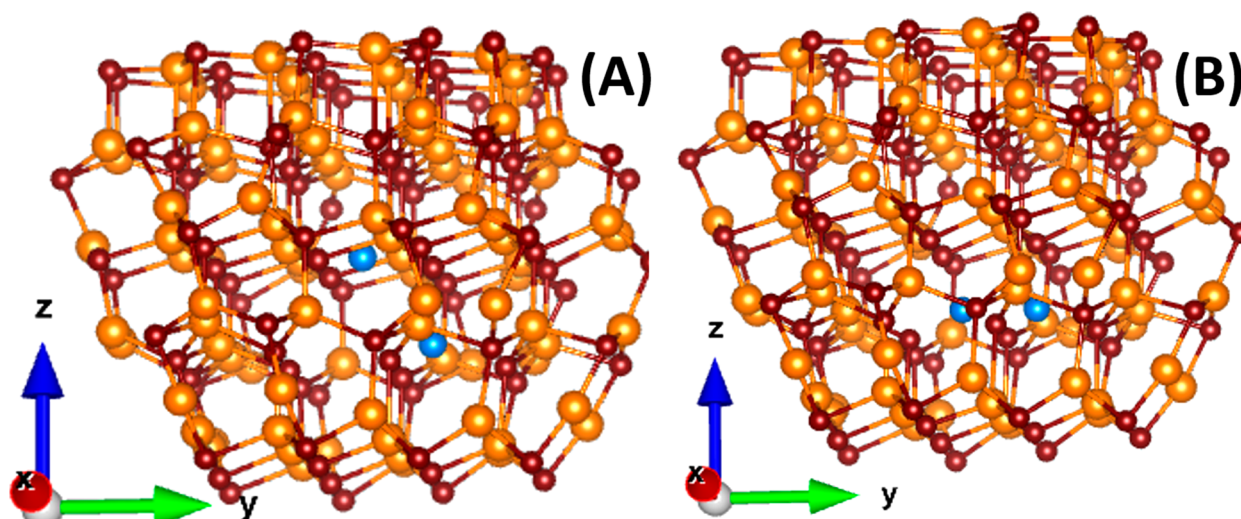
**Figure 6.** DFT predictions for the site of occupation for an Fe–Fe pair in $Cd_{87}Se_{90}Fe_2$. The blue atoms are Fe. The second Fe atom has moved down as seen in part B.

**Table 4. Barrier Energies for Diffusion of Fe(III) and Cd Ions**

| transitions | barrier energy (eV) |
|---|---|
| $Fe_{sub} \rightarrow Fe_{int}$[a] and $Cd_{int} \rightarrow Cd_{sub}$ | 0.02 |
| $Fe_{int} \rightarrow Fe_{int}$ | 0.28 |
| $Cd_{sub} \rightarrow Cd_{int}$ and $Fe_{int} \rightarrow Fe_{sub}$ | 0.55 |

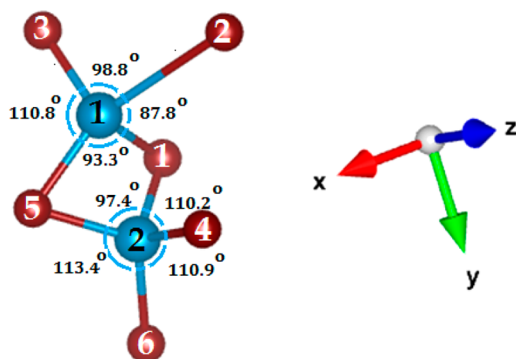[a]int stands for interstitial site, and sub stands for substitutional site.



**Figure 7.** Distorted tetrahedral interstitial site is occupied by Fe labeled 1. Brown atoms labeled 1–6 are Se, and the blue ones are Fe.

preference for tetrahedral sites and that they are unlikely to occupy [B] octahedral sites we arrive at $(\uparrow Fe_{0.8}Cd_{0.2})[\downarrow Fe_{1.2}\square_{0.8}]Se_4$ where $\square$ denotes a vacancy. The DFT calculations support the formation of the spin sublattices arising from formation of Fe(III) antisite pairs coupled to a $V_{Cd}$, indicating as the Fe concentration increases, ion clustering of the aliovalent ions likely produces magnetic inclusions. Such behavior has been suggested to occur for aliovalent doping of II–VI QDs previously.[32,33,35] More importantly the study reveals the underlying origin for RT-FM reported in II–VI QDs that have iron inclusions.

## ■ EXPERIMENTAL SECTION

**Chemicals.** Hexadecylamine (HDA) (90%, Acros Organics), $FeCl_2$ (99.9% Acros Organics), $^{57}Fe$ powder (Cambridge Isotopes), HCl (37%, Sigma-Aldrich), toluene (99.9%, EMD Chemicals), and methanol (99.8%, VWR) were used as supplied.

$Li_4[Se_4Cd_{10}(SC_6H_5)_{16}]$ ($Cd_{10}$ cluster) was prepared as previously described.[1]

**Synthesis.** Hexadecylamine (HDA) passivated Fe-doped CdSe QDs (~5 doping %) with a 0.2–0.6 nm size distribution were prepared by the reaction between the single-source precursor $Li_4[Se_4Cd_{10}(SC_6H_5)_{16}]$ ($Cd_{10}$) and $FeCl_2$ in HDA. Briefly, the QDs were prepared by the dissolution of 480 mg ($7.47 \times 10^{-5}$ mol) of $Cd_{10}$ in ~20 mL of HDA at 110 °C under $N_2$ using a Schlenk line. A 0.5 mg portion of $FeCl_2$ was added to the solution, and the reaction was allowed to stir vigorously for 1 h to induce metal exchange between the Cd(II) of the cluster and the Fe(III) from the metal salt. The reaction was then heated to 210 °C (5 °C/min) to induce QD growth. The temperature was kept below 220 °C to avoid sulfur incorporation, which has been seen in other studies.[41] The size of the QDs was monitored using UV–vis spectroscopy. Once the desired size was achieved the solution was cooled to room temperature to halt further growth. The cooled solid samples were then isolated by dissolving in ~10 mL of toluene, followed by precipitated with ~15 mL of MeOH, and centrifugation. This process was repeated three times to ensure reagent free particles, and the precipitate was dried under a vacuum at room temperature. Sequential dissolution/ precipitation steps have been shown to effectively remove unreacted Fe impurities. To generate $^{57}Fe$-doped CdSe for Mössbauer studies, $^{57}FeCl_2$ was used as the dopant source. The metal salt was synthesized using $^{57}Fe$ powder and HCl in MeOH.

The QD size and dispersion was analyzed by TEM for QDs dispersed on holey carbon (400 mesh) from a toluene solution using a JEOL-2010 microscope operated at 200 kV. The TEM measurements confirm the preliminary size obtained using absorption spectroscopy. Structural analysis and QD size was obtained using pXRD of 10 mg samples on a Rigaku DMAX 300 Ultima 3 powder X-ray diffractometer (using Cu K$\alpha$ $\lambda$ = 1.5418 Å radiation). The optical properties of QDs were analyzed using absorption spectra carried out on a Varian Cary 50 UV–vis spectrophotometer, and photoluminescence measurements were performed on a Varian Cary Eclipse florescence spectrophotometer. The Fe-doping level was analyzed by inductively coupled plasma mass spectrometry (ICP-MS) and was found to be ~4.6% for all samples.

**Magnetic Susceptibility Measurements.** Magnetization measurements were conducted on 5.1 nm, 4.6% Fe CdSe QDs using a Quantum Design superconducting quantum interference device (SQUID) magnetometer; zero-field cooled (ZFC) and field cooled (FC) measurements were performed under a constant field of 100 Oe over the temperature range 1.8–300 K. Isothermal field-dependent magnetization measurements were conducted with magnetic field varying between 0 and 7 T at 1.8 K.

**Electron Paramagnetic Resonance.** High-frequency EPR (HF-EPR), 240 GHz, measurements were conducted at the Florida State University National High Magnetic Field Laboratory (FSU-NHMFL) in Tallahassee, FL. The superheterodyne quasioptical spectrometer operates at 120, 240, and 336 GHz and is described elsewhere. A multifrequency high-field pulsed electron paramagnetic resonance/electron−nuclear double resonance spectrometer was used.[58,59] Spectral simulations were performed using the computer program EPRCALC.

**Mössbauer.** The $^{57}$Fe nuclear gamma resonance (Mössbauer) spectra were recorded using a spectrometer fitted with a Janis 8DT Super Varitemp flow-type cryostat cooled with liquid helium. The cryostat had a built in 8 T, American Magnetics superconducting magnet. The spectrometer was operated in a constant acceleration mode and used a light source that consisted of 100 mCi $^{57}$Co dispersed in Rh metal foil. This instrument allowed for recording spectra for temperatures 4.2−298 K and applied fields from 0 to 8 T at 4.2 K. The external field was applied parallel to the incident $\gamma$-radiation. The absorbers used in this study were obtained by dispersing 10−15 mg of Fe-doped CdSe QDs in ∼50 mg of eicosane that was gently warmed to 40 °C followed by cooling to room temperature (RT). This procedure allowed us to investigate samples that were magnetically dilute, which were solid at room temperature and thus were easy to handle. These absorbers were contained in custom-made Delrin or polyethylene containers. The large non-resonant absorption of the 14.4 keV photons by the Cd and Se nuclei required us to use $^{57}$Fe isotopically enriched absorbers. The isomer shift values are reported against the room-temperature centroid of a standard $\alpha$-Fe metal foil. The experimental spectra were analyzed using the WMOSS software (See Co., formerly Web Research Co., Edina, MN) in the framework of the Voigt-based model first described by Rancourt et al.[60] An arbitrary distribution of hyperfine fields (HFD) is described in terms of a sum of individual Gaussian components. Each component can originate from sum of elemental spectra that account for different values of the distributed parameters and have intensities that follow a Gaussian distribution. Each component is defined by three parameters, namely, $p$ [%], a weight factor (assuming identical $f$-recoilless fractions $p$ accounts for the fraction of the total Fe amount of the respective component); $\mathbf{B}_{obs}$ [T], the centroid; and d$B$ [T], the width of the Gaussian HFD. In zero-field the $\mathbf{B}_{obs}$ [T] denotes the $B_0$ of the respective component. The parameters used to describe the sextet spectra used to represent the HFD are $\Gamma$, the full width at half-maximum (fwhm) of the intrinsic Lorentzian line-shape; $\delta$, the isomer shift; $\varepsilon$, the electric field gradient (EFG) tensor component along the internal field; and $h_1/h_3$ and $h_2/h_3$, the intensity ratios of the outer (1, 6) lines to the inner (3, 4) lines and of the middle (2, 5) lines to the inner (3, 4) lines, respectively.

**DFT Computational Methods.** The charge of the Fe(III) is set in VASP by varying the total number of valence electrons of the nanocluster. A compensating background charge is added automatically to neutralize the system. The nanoclusters are grown in a colloid and are considered to be in contact with particle reservoirs of Cd, Fe, and Se. The computations were performed with projector augmented wave (PAW) pseudopotentials with default energy cut-offs of 205.744 eV for Cd, 200.930 eV for Fe, and 158.668 eV for Se using the generalized gradient approximation of Perdew and Wang (PW91) for the exchange correlation function.[61] The supercell computations were generated in reciprocal space with $\gamma$ point for Brillouin-zone integration. A vacuum region of 12 Å was placed around the cluster to avoid interaction with periodic images. A conjugant gradient geometry optimization was applied until a convergence criterion of 0.025 eV/Å or less for forces on the ions was obtained. A lower convergence criterion was tried, but the computations did not converge at accurate level of precision for such a large cluster.

## ASSOCIATED CONTENT

**ⓢ Supporting Information**

The Supporting Information is available free of charge on the ACS Publications website at DOI: 10.1021/acs.chemmater.8b02505.

Further details of DFT-GGA computational methods, magnetic data, and Mössbauer data (PDF)

## AUTHOR INFORMATION

**Corresponding Author**

*E-mail: strouse@chem.fsu.edu.

**ORCID**

Jasleen K. Bindra: 0000-0001-7031-7482
Naresh S. Dalal: 0000-0002-9996-6918
Sebastian A. Stoian: 0000-0003-3362-7697
Geoffrey F. Strouse: 0000-0003-0841-282X

**Author Contributions**

The manuscript was written through contributions of all authors. All authors have given approval to the final version of the manuscript. J.K.B. prepared and measured the properties of the synthesized QD. G.K. and M.D.M. performed the DFT calculations. S.A.S. carried out the Mössbauer measurements. J.V.T. performed EPR measurements. N.S.D. analyzed the EPR and magnetic properties. G.F.S. designed the project, and assisted in interpretation, conclusions, and in the writing of the manuscript.

**Notes**

The authors declare no competing financial interest.

## REFERENCES

(1) Cumberland, S. L.; Hanif, K. M.; Javier, A.; Khitrov, G. A.; Strouse, G. F.; Woessner, S. M.; Yun, C. S. Inorganic clusters as single-source precursors for preparation of CdSe, ZnSe, and CdSe/ZnS nanomaterials. *Chem. Mater.* **2002**, *14*, 1576−1584.

(2) Archer, P. I.; Santangelo, S. A.; Gamelin, D. R. Inorganic cluster syntheses of TM$^{2+}$-doped quantum dots (CdSe, CdS, CdSe/CdS): physical property dependence on dopant locale. *J. Am. Chem. Soc.* **2007**, *129*, 9808−9818.

(3) Norman, T. J.; Magana, D.; Wilson, T.; Burns, C.; Zhang, J. Z.; Cao, D.; Bridges, F. Optical and surface structural properties of Mn$^{2+}$-doped ZnSe nanoparticles. *J. Phys. Chem. B* **2003**, *107*, 6309−6317.

(4) Son, D. H.; Hughes, S. M.; Yin, Y.; Alivisatos, A. P. Cation exchange reactions in ionic nanocrystals. *Science* **2004**, *306*, 1009−1012.

(5) Vlaskin, V. A.; Barrows, C. J.; Erickson, C. S.; Gamelin, D. R. Nanocrystal diffusion doping. *J. Am. Chem. Soc.* **2013**, *135*, 14380−14389.

(6) Barrows, C. J.; Vlaskin, V. A.; Gamelin, D. R. Absorption and Magnetic Circular Dichroism Analyses of Giant Zeeman Splittings in Diffusion-Doped Colloidal $Cd_{1-x}$ $Mn_x$ Se Quantum Dots. *J. Phys. Chem. Lett.* **2015**, *6*, 3076−3081.

(7) Ha, D. H.; Caldwell, A. H.; Ward, M. J.; Honrao, S.; Mathew, K.; Hovden, R.; Koker, M. K.; Muller, D. A.; Hennig, R. G.; Robinson, R. D. Solid−Solid Phase Transformations Induced through Cation Exchange and Strain in 2D Heterostructured Copper Sulfide Nanocrystals. *Nano Lett.* **2014**, *14*, 7090−7099.

(8) Radovanovic, P. V.; Gamelin, D. R. High-Temperature Ferromagnetism in $Ni^{2+}$-Doped ZnO Aggregates Prepared from Colloidal Diluted Magnetic Semiconductor Quantum Dots. *Phys. Rev. Lett.* **2003**, *91*, 157202−157206.

(9) Wolf, S. A.; Awschalom, D. D.; Buhrman, R. A.; Daughtton, J. M.; Molnar, S. v.; Roukes, M. L.; Chtchelkanova, A. Y.; Treger, D. M. Spintronics: a spin-based electronics vision for the future. *Science* **2001**, *294*, 1488−1495.

(10) Erwin, S. C.; Zu, L.; Haftel, M. I.; Efros, A. L.; Kennedy, T. A.; Norris, D. J. Doping Semiconductor Nanocrystals. *Nature* **2005**, *436*, 91−94.

(11) Jaworski, M. C.; Yang, J.; Mack, S.; Awschalom, D. D.; Heremans, J. P.; Myers, R. C. Observation of the Spin-Seebeck Effect in a Ferromagnetic Semiconductor. *Nat. Mater.* **2010**, *9*, 898−903.

(12) Mittleman, D. M.; Schoenlein, R. W.; Shiang, J. J.; Colvin, V. L.; Alivisatos, A. P.; Shank, C. V. Quantum size dependence of femtosecond electronic dephasing and vibrational dynamics in CdSe nanocrystals. *Phys. Rev. B: Condens. Matter Mater. Phys.* **1994**, *49*, 14435−14447.

(13) Peng, X.; Schlamp, M. C.; Kadavanich, A. V.; Alivisatos, A. P. Epitaxial growth of highly luminescent CdSe/CdS core/shell nanocrystals with photostability and electronic accessibility. *J. Am. Chem. Soc.* **1997**, *119*, 7019−7029.

(14) Beaulac, R.; Archer, P. I.; Ochsenbein, S. T.; Gamelin, D. R. $Mn^{2+}$ Doped CdSe Quantum Dots: New Inorganic Materials for Spin-Electronics and Spin-Photonics. *Adv. Funct. Mater.* **2008**, *18*, 3873−3891.

(15) Luther, J. M.; Jain, P. K.; Ewers, T.; Alivisatos, A. P. Localized surface plasmon resonances arising from free carriers in doped quantum dots. *Nat. Mater.* **2011**, *10*, 361−366.

(16) Pacifici, D.; Lezec, H. J.; Atwater, H. A. All-optical modulation by plasmonic excitation of CdSe quantum dots. *Nat. Photonics* **2007**, *1*, 402−406.

(17) Jin, Y.; Gao, X. Plasmonic fluorescent quantum dots. *Nat. Nanotechnol.* **2009**, *4*, 571−576.

(18) Garcia, G.; Buonsanti, R.; Runnerstrom, E. L.; Mendelsberg, R. J.; Llordes, A.; Anders, A.; Richardson, T. J.; Milliron, D. J. Dynamically modulating the surface plasmon resonance of doped semiconductor nanocrystals. *Nano Lett.* **2011**, *11*, 4415−4420.

(19) Strouse, G. F.; Schoonover, J. R.; Duesing, R.; Boyde, S.; Jones, W. E. J.; Meyer, T. J. Influence of electronic delocalization in metal-to-ligand charge transfer excited states. *Inorg. Chem.* **1995**, *34*, 473−487.

(20) Beaulac, R.; Schneider, L.; Archer, P. I.; Bacher, G.; Gamelin, D. R. Light-induced spontaneous magnetization in doped colloidal quantum dots. *Science* **2009**, *325*, 973−976.

(21) Santra, P. K.; Kamat, P. V. Mn-doped quantum dot sensitized solar cells: a strategy to boost efficiency over 5%. *J. Am. Chem. Soc.* **2012**, *134*, 2508−2511.

(22) Fainblat, R.; Barrows, C. J.; Gamelin, D. R. Single Magnetic Impurities in Colloidal Quantum Dots and Magic-Size Clusters. *Chem. Mater.* **2017**, *29*, 8023−8036.

(23) Schimpf, A. M.; Ochsenbein, S. T.; Gamelin, D. R. Surface Contributions to $Mn^{2+}$ Spin Dynamics in Colloidal Doped Quantum Dots. *J. Phys. Chem. Lett.* **2015**, *6*, 457−63.

(24) Zheng, W.; Wang, Z.; Wright, J.; Goundie, B.; Dalal, N. S.; Meulenberg, R. W.; Strouse, G. F. Probing the Local Site Environments in Mn: CdSe Quantum Dots. *J. Phys. Chem. C* **2011**, *115*, 23305−23314.

(25) Magana, D.; Perera, S. C.; Harter, A. G.; Dalal, N. S.; Strouse, G. F. Switching-on Superparamagnetism in Mn/CdSe Quantum Dots. *J. Am. Chem. Soc.* **2006**, *128*, 2931−2939.

(26) Zheng, W.; Strouse, G. F. Involvement of Carriers in the Size-Dependent Magnetic Exchange for Mn: CdSe Quantum Dots. *J. Am. Chem. Soc.* **2011**, *133*, 7482−7489.

(27) Hanif, K. M.; Meulenberg, R. W.; Strouse, G. F. Magnetic Ordering in Doped $Cd_{1-x}Co_xSe$ Diluted Magnetic Quantum Dots. *J. Am. Chem. Soc.* **2002**, *124*, 11495−11502.

(28) Radovanovic, P. V.; Gamelin, D. R. Electronic Absorption Spectroscopy of Cobalt Ions in Diluted Magnetic Semiconductor Quantum Dots: Demonstration of an Isocrystalline Core/Shell Synthetic Method. *J. Am. Chem. Soc.* **2001**, *123*, 12207−12214.

(29) Kittilstved, K. R.; Schwartz, D. A.; Tuan, A. C.; Heald, S. M.; Chambers, S. A.; Gamelin, D. R. Direct Kinetic Correlation of Carriers and Ferromagnetism in $Co^{2+}$: ZnO. *Phys. Rev. Lett.* **2006**, *97*, 037203−037207.

(30) Zhou, D.; Kittilstved, K. R. Control over $Fe^{3+}$ Speciation in Colloidal ZnO Nanocrystals. *J. Mater. Chem. C* **2015**, *3*, 4352−4358.

(31) Zhou, D.; Kittilstved, K. R. Electron Trapping on $Fe^{3+}$ Sites in Photodoped ZnO Colloidal Nanocrystals. *Chem. Commun.* **2016**, *52*, 9101−9104.

(32) Zheng, W.; Singh, K.; Wang, Z.; Wright, J. T.; van Tol, J.; Dalal, N. S.; Meulenberg, R. W.; Strouse, G. F. Evidence of a $ZnCr_2Se_4$ Spinel Inclusion at the Core of a Cr-Doped ZnSe Quantum Dot. *J. Am. Chem. Soc.* **2012**, *134*, 5577−5585.

(33) Foley, M. E.; Meulenberg, R. W.; McBride, J. R.; Strouse, G. F. $Eu^{3+}$-doped $ZnB_2O_4$ (B = $Al^{3+}$, $Ga^{3+}$) Nanospinels: An Efficient Red Phosphor. *Chem. Mater.* **2015**, *27*, 8362−8364.

(34) Hanif, K. M.; Strouse, G. F. Synthesis and Characterization of $Cd_{1-x}$ $Cu_x$ Se Quantum Dots. *MRS Online Proc. Libr.* **2003**, *789*, 431−432.

(35) Bindra, J. K.; Gutsev, L. G.; Van Tol, J.; Singh, K.; Dalal, N. S.; Strouse, G. F. Experimental Validation of Ferromagnetic-Antiferromagnetic Competition in $Fe_xZn_{1-x}Se$ Quantum Dots by Computational Modelling. *Chem. Mater.* **2018**, *30*, 2093−2101.

(36) Singh, S. B.; Limaye, M. V.; Date, S. K.; Gokhale, S.; Kulkarni, S. K. Iron Substitution in CdSe Nanoparticles: Magnetic and Optical Properties. *Phys. Rev. B: Condens. Matter Mater. Phys.* **2009**, *80*, 235421−235429.

(37) Saha, A.; Viswanatha, R. Volume and Concentration Scaling of Magnetism in Dilute Magnetic Semiconductor Quantum Dots. *J. Phys. Chem. C* **2017**, *121*, 21790−21796.

(38) Karmakar, D.; Mandal, S. K.; Kadam, R. M.; Paulose, P. L.; Rajarajan, A. K.; Nath, T. K.; Das, A. K.; Dasgupta, I.; Das, G. P. Ferromagnetism in Fe-Doped ZnO Nanocrystals: Experiment and Theory. *Phys. Rev. B: Condens. Matter Mater. Phys.* **2007**, *75*, 144404−144418.

(39) Tian, J. H.; Song, T.; Sun, X. W.; Wang, T.; Jiang, G. First-Principles Study on the Half-Metallic Ferromagnetism and Optical Properties of Fe-Doped CdSe and Co-Doped CdSe. *J. Supercond. Novel Magn.* **2017**, *30*, 521−528.

(40) Tomiyasu, K.; Kamazawa, K. A Spin Molecule Model for Geometrically Frustrated Spinel $ZnFe_2O_4$. *J. Phys. Soc. Jpn.* **2011**, *80*, SB024−3.

(41) Lovingood, D. D.; Oyler, R. E.; Strouse, G. F. Composition Control and Localization of $S^{2-}$ in CdSSe Quantum Dots Grown from $Li_4[Cd_{10}Se_4(SPh)_{16}]$. *J. Am. Chem. Soc.* **2008**, *130*, 17004−170011.

(42) Vegard, L. The constitution of the mixed crystals and the space filling of the atoms. *Eur. Phys. J. A* **1921**, *5*, 17−26.

(43) Singhal, A.; Achary, S. N.; Manjanna, J.; Jayakumar, O. D.; Kadam, R. M.; Tyagi, A. K. Colloidal Fe-Doped Indium Oxide Nanoparticles: Facile Synthesis, Structural, and Magnetic Properties. *J. Phys. Chem. C* **2009**, *113*, 3600−3606.

(44) Watanabe, H. g-value of $Fe^{3+}$ in II−VI Cubic Crystals. *J. Phys. Chem. Solids* **1964**, *25*, 1471−1475.

(45) Morup, S.; Dumesic, J. A.; Topsoe, H. *Applications of Mössbauer Spectroscopy*; Cohen, R. L., Ed.; Academic Press: New York, 1980.

(46) Morup, S.; Hansen, M. F. *Handbook of Magnetism and Advanced Magnetic Materials*; Kronmueller, H., Parkin, S., Eds.; John Wiley and Sons, Ltd.: New York, 2007.

(47) Gütlich, P.; Bill, E.; Trautwein, A. X. *Mössbauer Spectroscopy and Transition Metal Chemistry*; Springer-Verlag: Lubeck-Germany, 2011.

(48) Mörup, S.; Tronc, E. Superparamagnetic Relaxation of Weakly Interacting Particles. *Phys. Rev. Lett.* **1994**, *72*, 3278−3281.

(49) Blanco-Gutiérrez, V.; Gallastegui, J. A.; Bonville, P.; Torralvo-Fernández, M. J.; Sáez-Puche, R. $MFe_2O_4$ (M: $Co^{2+}$, $Ni^{2+}$) Nanoparticles: Mössbauer and X-ray Absorption Spectroscopies Studies and High-Temperature Superparamagnetic Behavior. *J. Phys. Chem. C* **2012**, *116*, 24331−24339.

(50) Kresse, G.; Hafner, J. Norm-Conserving and Ultrasoft Pseudopotentials for First-Row and Transition Elements. *J. Phys.: Condens. Matter* **1994**, *6*, 8245−8257.

(51) Kresse, G.; Furthmüller, J. Efficient Iterative Schemes for ab Initio Total-Energy Calculations Using a Plane-Wave Basis Set. *Phys. Rev. B: Condens. Matter Mater. Phys.* **1996**, *54*, 11169−11186.

(52) Van de Walle, C. G.; Neugebauer, J. First-Principles Calculations for Defects and Impurities: Application to III-nitrides. *J. Appl. Phys.* **2004**, *95*, 3851−3879.

(53) Ott, F. D.; Spiegel, L. L.; Norris, D. J.; Erwin, S. C. Microscopic theory of cation exchange in CdSe nanocrystals. *Phys. Rev. Lett.* **2014**, *113*, 156803.

(54) Shaw, D. *Widegap II-VI Compounds for Opto-Electronic Applications*; Ruda, H. E., Ed.; Chapman Hall: London, 1992.

(55) Sullivan, C. J. L. An ultrasonic study of the diffusion of Ag in CdSe in the temperature range 20°−400°. *Thin Solid Films* **1975**, *25*, 245−251.

(56) Dalpian, G. M.; Chelikowsky, J. R. Self-purification in Semiconductor Nanocrystals. *Phys. Rev. Lett.* **2006**, *96*, 226802−226806.

(57) The importance of Coulomb interaction is pointed in ref 54.

(58) Morley, G. W.; Brunel, L. C.; van Tol, J. A Multifrequency High-Field Pulsed Electron Paramagnetic Resonance/Electron-Nuclear Double Resonance Spectrometer. *Rev. Sci. Instrum.* **2008**, *79*, 064703−064705.

(59) Van Tol, J.; Brunel, L.-C.; Wylde, R. J. A Quasioptical Transient Electron Spin Resonance Spectrometer Operating at 120 and 240 GHz. *Rev. Sci. Instrum.* **2005**, *76*, 074101−0741019.

(60) Rancourt, D. G.; Ping, J. Y. Voigt-based Methods for Arbitrary-Shape Static Hyperfine Parameter Distributions in Mössbauer Spectroscopy. *Nucl. Instrum. Methods Phys. Res., Sect. B* **1991**, *58*, 85−97.

(61) Perdew, J. P.; Wang, Y. Accurate and Simple Analytic Representation of the Electron-Gas Correlation Energy. *Phys. Rev. B: Condens. Matter Mater. Phys.* **1992**, *45*, 13244−13249.